INTERNATIONAL JOURNAL FOR NUMERICAL METHODS IN ENGINEERING, VOL. 37, 2569–2582 (1994)

A SIMPLE TRIANGULAR ELEMENT FOR THICK AND THIN PLATE AND SHELL ANALYSIS

E. OÑATE, F. ZARATE AND F. FLORES

International Center for Numerical Methods in Engineering, E.T.S. Ingenieros de Caminos, Canales y Puertos, Univ. Politécnica de Cataluña, Gran Capitán s/n, 08034 Barcelona, Spain

SUMMARY

A new plate triangle based on Reissner–Mindlin plate theory is proposed. The element has a standard linear deflection field and an incompatible linear rotation field expressed in terms of the mid-side rotations. Locking is avoided by introducing an assumed linear shear strain field based on the tangential shear strains at the mid-sides. The element is free of spurious modes, satisfies the patch test and behaves correctly for thick and thin plate and shell situations. The element degenerates in an explicit manner to a simple discrete Kirchhoff form.

INTRODUCTION

Considerable effort has been put in recent years in the development of C_0 continuous plate and shell elements valid for both thick and thin situations. A survey of recent work in this direction can be found in References 1–4. Despite all these efforts there are not many elements that satisfy all the following 'optimum' requirements:

(a) proper rank (no spurious modes for one element)
(b) no shear locking
(c) satisfaction of constant curvature patch tests
(d) low sensitivity to distortions
(e) good accuracy in displacements and stresses for thin and thick situations
(f) non-dependence of artificial numerical factors
(g) simplicity of the formulation and of the programming

This paper presents a new triangular element which satisfies most (if not all) of the above requirements. The displacement field is described by a standard C_0 linear interpolation of the deflection in terms of the three corner values and a linear interpolation of the rotations in terms of the mid-side rotations. This introduces an incompatibility of the normal rotation along the sides of adjacent elements which, however, does not preclude satisfaction of the patch test. Shear locking is avoided by means of an assumed linear shear strain field in terms of the (constant) tangential shear values at the element mid-sides. This ensures fulfilment of the necessary compatibility conditions between the deflection, rotation and shear fields to guarantee the absence of locking in the thin limit.[1–3,5–7]

The layout of the paper is the following. The basic equations of Reissner–Mindlin plate theory are briefly presented first. The finite element interpolation used is described next together with details of the derivation of the curvature and shear strain matrices. Examples of the good performance of the element proposed are presented for a range of plate and shell problems. The

CCC 0029–5981/94/152569–14$9.00

Received 6 October 1993

degeneration of the element to a simpler discrete Kirchhoff (DK) form involving three corner deflection values and three mid-side normal rotations is also briefly shown.

BASIC EQUATIONS OF REISSNER–MINDLIN PLATE THEORY

Figure 1 shows the geometry of a plate with the sign convention for the deflection w and the two independent rotations θ_x, θ_y.

Table 1 shows the basic equations of Reissner–Mindlin plate theory[1,2] defining the curvature and shear strain fields, the constitutive relationships and the equilibrium equation for a distributed loading q expressed by the Principle of Virtual Work (PVW).

FINITE ELEMENT INTERPOLATION

Figure 2 shows the geometry of the triangular element proposed. The deflection field is linearly interpolated in terms of the three corner deflection values as

$$w = \sum_{i=1}^{3} L_i w_i \tag{1}$$

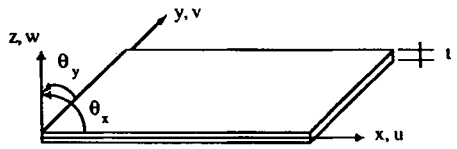

Figure 1. Sign convention for displacement and rotations in a plate

Table 1. Basic equations of Reissner–Mindlin plate theory

Displacement field

$$\mathbf{u} = [w, \boldsymbol{\theta}^{\mathrm{T}}]^{\mathrm{T}}, \quad \boldsymbol{\theta} = [\theta_x, \theta_y]^{\mathrm{T}}$$

Curvature field

$$\boldsymbol{\chi} = [\chi_x, \chi_y, \chi_{xy}]^{\mathrm{T}} = \left[-\frac{\partial \theta_x}{\partial x}, -\frac{\partial \theta_y}{\partial y}, -\left(\frac{\partial \theta_x}{\partial y} + \frac{\partial \theta_y}{\partial x}\right)\right]^{\mathrm{T}}$$

Shear strain field

$$\boldsymbol{\gamma} = [\gamma_x, \gamma_y]^{\mathrm{T}} = \left[\frac{\partial w}{\partial x} - \theta_x, \frac{\partial w}{\partial y} - \theta_y\right]^{\mathrm{T}}$$

Constitutive relationships

$$\mathbf{m} = [m_x, m_y, m_{xy}]^{\mathrm{T}} = \mathbf{D}_{\mathrm{b}}\boldsymbol{\chi}$$

$$\mathbf{s} = [Q_x, Q_y]^{\mathrm{T}} = \mathbf{D}_{\mathrm{s}}\boldsymbol{\gamma}$$

$$\mathbf{D}_{\mathrm{b}} = \frac{Et^3}{12(1-\nu^2)}\begin{bmatrix} 1 & \nu & 0 \\ \nu & 1 & 0 \\ 0 & 0 & (1-\nu)/2 \end{bmatrix}, \quad \mathbf{D}_{\mathrm{s}} = \alpha G t \begin{bmatrix} 1 & 0 \\ 0 & 1 \end{bmatrix}, \quad \alpha = 5/6$$

Principle of virtual work

$$\iint_A [\delta\boldsymbol{\chi}^{\mathrm{T}}\mathbf{m} + \delta\boldsymbol{\gamma}^{\mathrm{T}}\mathbf{s}]\, \mathrm{d}A = \iint_A \delta w q\, \mathrm{d}A$$

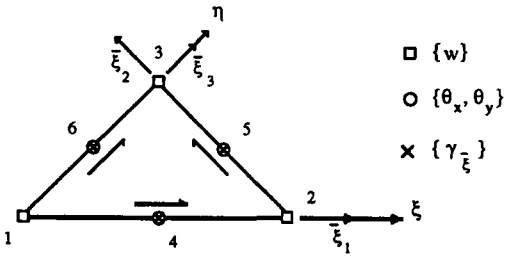

Figure 2. Geometric description and nodal variables of the TLLL plate element

where $L_1 = 1 - \xi - \eta$, $L_2 = \xi$ and $L_3 = \eta$ are the shape functions of the standard linear triangle.[1,2]

The rotation field is linearly interpolated in terms of the rotations at the element mid-sides as

$$\boldsymbol{\theta} = \sum_{i=4}^{6} N_i \boldsymbol{\theta}_i, \quad \boldsymbol{\theta}_i = [\theta_{xi}, \theta_{yi}]^T \tag{2}$$

where

$$N_4 = 1 - 2\xi, \quad N_5 = 2\xi + 2\eta - 1, \quad N_6 = 1 - 2\eta \tag{3}$$

are the linear shape functions of nodes 4, 5 and 6.

Equations (2) and (3) define an incompatible rotation field with side continuity enforced at the mid-side nodes only. The good performance of the element, in ensured via satisfaction of the patch test as shown in the next section.

Curvature matrix

Substituting (2) into the curvature–rotation relationship of Table I leads to

$$\boldsymbol{\chi} = \mathbf{B}_b \mathbf{a} \tag{4}$$

with the nodal displacement vector defined as

$$\mathbf{a} = [w_1, w_2, w_3, \theta_{x4}, \theta_{y4}, \theta_{x5}, \theta_{y5}, \theta_{x6}, \theta_{y6},]^T \tag{5}$$

and the curvature matrix given by

$$\mathbf{B}_b = [\underset{3\times 3}{0}, \mathbf{B}_{b_4}, \mathbf{B}_{b_5}, \mathbf{B}_{b_6},], \quad \mathbf{B}_{b_i} = \begin{bmatrix} -\partial N_i/\partial x & 0 \\ 0 & -\partial N_i/\partial y \\ -\partial N_i/\partial y & -\partial N_i/\partial x \end{bmatrix} \tag{6}$$

Note that $\mathbf{B}_{b_i}$ is constant for straight sided triangles.

Shear strain matrix

The assumed shear strain field is expressed in terms of the three tangential shear strains at the element mid-side points. After some algebra we can write in the natural co-ordinate system[7]

$$\boldsymbol{\gamma}' = \begin{Bmatrix} \gamma_\xi \\ \gamma_\eta \end{Bmatrix} = \begin{bmatrix} 1-\eta & -\eta\sqrt{2} & \eta \\ \xi & \xi\sqrt{2} & 1-\xi \end{bmatrix} \begin{Bmatrix} \gamma_{\bar{\xi}_1} \\ \gamma_{\bar{\xi}_2} \\ \gamma_{\bar{\xi}_3} \end{Bmatrix} = \mathbf{A}\hat{\boldsymbol{\gamma}}_{\bar{\xi}} \tag{7}$$

where $\gamma_{\bar{\xi}_1}$, $\gamma_{\bar{\xi}_2}$, and $\gamma_{\bar{\xi}_3}$, are the tangential shear strains along sides 1–2, 2–3 and 1–3, respectively. The signs of the elements of matrix **A** in (7) correspond to the directions of side co-ordinates $\bar{\xi}_1$, $\bar{\xi}_2$, and $\bar{\xi}_3$, as shown in Figure 2.[7,8]

This shear strain interpolation coincides precisely with that used for the linear/quadratic plate triangles in References 6 and 7. It can be easily checked that the chosen displacement and shear fields satisfy the *necessary conditions* for avoidance of locking defined as $n_w + n_\theta \geqslant n_\gamma$ and $n_\gamma \geqslant n_w$, where n_w, n_θ and n_γ are the number of available deflection, rotation and shear strain variables (after discounting the prescribed values). Further details on the variational justification of these inequalities can be found in References 1, 2, 4–7.

The shear strain–displacement relationship is obtained by imposing along each side the condition $\gamma_{\bar{\xi}} - (\partial w/\partial\bar{\xi} - \theta_{\bar{\xi}}) = 0$ to be satisfied in a weighted integral form as

$$\int_{l_{ij}} W\left[\gamma_{\bar{\xi}} - \frac{\partial w}{\partial \bar{\xi}} + \theta_{\bar{\xi}}\right] \mathrm{d}\bar{\xi} = 0 \tag{8}$$

The choice of a constant interpolation of the tangential shear strain along each side and a Galerkin weighting ($W = 1$) leads after appropriate substitution of (1) and (2) into (8) to

$$\hat{\boldsymbol{\gamma}}_{\bar{\xi}} = \begin{Bmatrix} \gamma_{\bar{\xi}_1} \\ \gamma_{\bar{\xi}_2} \\ \gamma_{\bar{\xi}_3} \end{Bmatrix} = \begin{bmatrix} -1 & 1 & 0 & x_{12} & y_{12} & 0 & 0 & 0 & 0 \\ 0 & -1/\sqrt{2} & 1/\sqrt{2} & 0 & 0 & x_{23}/\sqrt{2} & y_{23}/\sqrt{2} & 0 & 0 \\ -1 & 0 & 1 & 0 & 0 & 0 & 0 & x_{13} & y_{13} \end{bmatrix} \mathbf{a} = \mathbf{C}\mathbf{a} \tag{9}$$

where $x_{ij} = x_i - x_j$, $y_{ij} = y_i - y_j$.

Combining (9) and (8) gives finally

$$\begin{Bmatrix} \gamma_x \\ \gamma_y \end{Bmatrix} = \mathbf{J}^{-1} \begin{Bmatrix} \gamma_\xi \\ \gamma_\eta \end{Bmatrix} = \mathbf{J}^{-1}\mathbf{A}\mathbf{C}\mathbf{a} = \bar{\mathbf{B}}_s\mathbf{a} \tag{10}$$

where **J** is the Jacobian matrix and

$$\bar{\mathbf{B}}_s = \mathbf{J}^{-1}\mathbf{A}\mathbf{C} \tag{11}$$

is the substitute shear strain matrix.[2,7]

Stiffness matrix and equivalent nodal force vector

Substitution of (5) and (11) in the PVW expression of Table I leads to the standard form of the element stiffness matrix as

$$\mathbf{K}^{(e)} = \mathbf{K}_b^{(e)} + \mathbf{K}_s^{(e)} \tag{12}$$

where the bending and shear contributions are given by

$$\mathbf{K}_b^{(e)} = \iint_{A^{(e)}} \mathbf{B}_b^{\mathrm{T}}\mathbf{D}_b\mathbf{B}_b \,\mathrm{d}A \tag{13}$$

$$\mathbf{K}_s^{(e)} = \iint_{A^{(e)}} \mathbf{B}_s^{\mathrm{T}}\mathbf{D}_s\mathbf{B}_s \,\mathrm{d}A \tag{14}$$

The expression of the equivalent nodal force vector for a distributed loading of intensity q is given by

$$\mathbf{f}_b^{(e)} = \iint_{A^{(e)}} \mathbf{N}^T q \, dA \quad \text{with} \quad \underset{3\times 9}{\mathbf{N}} = \begin{bmatrix} L_1 & L_2 & L_3 & \mathbf{0} \\ & \mathbf{0} & & \mathbf{0} \end{bmatrix} \tag{15}$$

Following the notation proposed in Reference 7 the thick plate element presented here will be termed TLLL (for Triangle with Linear interpolation for the deflection, rotations and shear strain fields).

Remark 1. The exact integration of $\mathbf{K}_b^{(e)}$ and $\mathbf{K}_s^{(e)}$ for straight side triangles and homogeneous material requires one and three integration points, respectively.

Remark 2. Special care must be taken to handle the different number of degrees of freedom per node at equation solution and pre- and postprocessing levels. Also the *a posteriori* computation of the rotation at corner nodes from the mid-side values for postprocessing purposes requires an adequate smoothing due to the incompatibility of the rotation field. Excellent results have been obtained in all cases by the authors using a simple nodal averaging procedure.

EXAMPLES

The performance of the TLLL plate element will be tested next for a number of plate problems.

Example 1. Study of element rank

An eigenvalue analysis shows that the element stiffness matrix, when exactly integrated, has only three zero eigenvalues for the whole range of thick and thin situations. The correctness of the element rank with respect to spurious mechanisms is therefore ensured.

The use of a reduced single point quadrature for the shear stiffness matrix introduces an extra zero eigenvalue. This invalidates, in principle, the use of this attractive simple quadrature for practical purposes. Preliminary numerical experiments show that this zero energy mode does not propagate in a mesh, leading to accurate and very economical solutions. This encouraging result should be further validated before any definitive conclusion can be drawn. Exact integration is therefore used in all examples presented next.

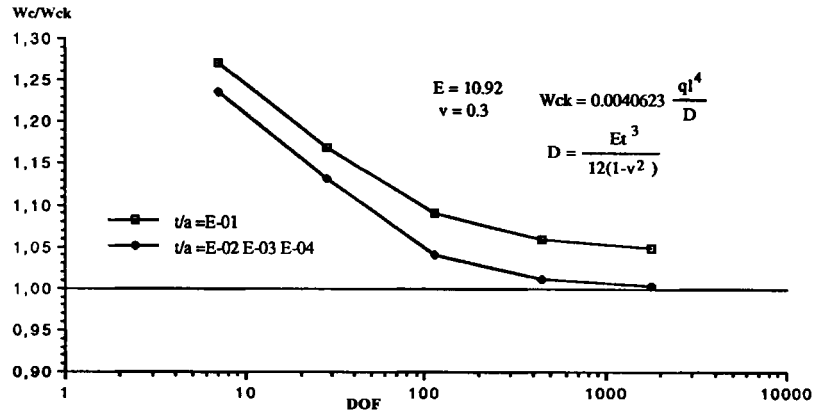

Figure 3. Convergence of normalized central deflection value for thick and thin situations in a simply supported square plate under uniform loading.

Example 2. Study of locking behaviour

Figure 3 shows the convergence of the central deflection value (normalized versus Kirchhoff's solution) for a simple supported square plate ($a \times a$) under uniform loading. The same convergence curve is obtained for a range of thicknesses from thick to very thin situations. Similar results have been obtained for different plate problems (i.e., rectangular, circular, skew, etc.) with different boundary conditions, thus verifying the absence of locking defects, as expected.

Example 3. Patch tests

The following patch tests have been analysed:

(a) *Constant bending moment test* (Figure 4(a): A constant bending moment field ($M_x = M_y = M_{xy} = 1$) is obtained in all elements for this relatively thin case, as expected.
(b) *Cantilever plate under constant bending moment* (Figure 4(b)): The element patch shown in Figure 4(b) with adequate boundary conditions was analysed. The correct constant bending moment field and central deflection value were obtained (see Figure 4(b)).
(c) *Twisting of a square plate* (Figure 4(c)): We consider a thin square plate supported at three corners and subjected to a concentrated load at the fourth corner. Excellent agreement with the exact solution was obtained for all meshes analysed (see Figure 4(c)).
(d) *Constant shear patch test* (Figure 4(d)): The geometry and boundary conditions for this patch test are shown in Figure 4(d). A constant moment and shear field is obtained in the whole domain, as expected.

Further details on the patch tests for the TLLL element can be found in Reference 8.

Example 4. Simply supported and clamped square plates under uniform loading

Table II shows the convergence of the central deflection and central bending moment M_x for thick ($t/a = 0{\cdot}1$) and thin ($t/a = 0{\cdot}01$) situations for a square plate with hard simple support conditions ($w = \theta_s = 0$). Numerical results are given for the two mesh orientations A and B shown in Figure 5. The same type of results are shown in Table III for the soft support ($w = 0$) case.

Table IV shows the convergence of the central deflection and central bending moment for the clamped case. Good results for thick and thin situations are obtained.

Example 5. Simply supported and clamped circular plates under uniform loading

Table V shows the convergence of the central deflection and central bending moment for circular plates with simply supported (soft: $w = 0$) and clamped edges. Good convergence to existing analytical solutions[9] is obtained for thick and thin situations.

Example 6: Cantilever skew plates under uniform loading

Table VI shows the convergence of the central deflections at the two free corners (Figure 5) for different cantilever skew plates under uniform loading. Good convergence to the numerical solutions obtained with alternative triangular elements[10,11] is obtained in all cases. Note, however, that the element shows a slightly stiffer behaviour than the elements presented in these references (in particular for high skew angles). This is compensated by the higher simplicity of the element proposed here.

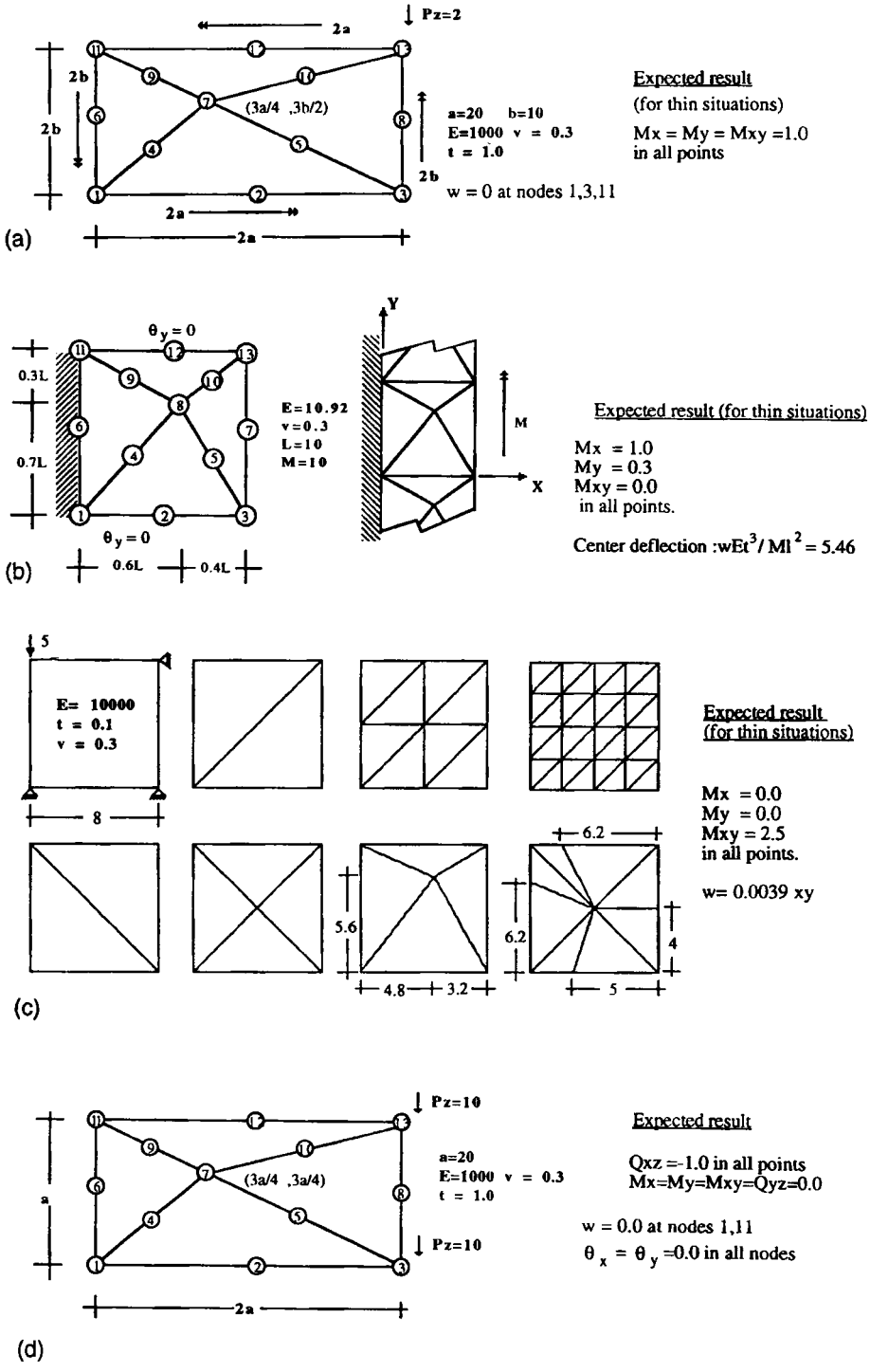

Figure 4. Patch tests for the TLLL element: (a) constant bending moment test; (b) cantilever plate under constant bending moment; (c) square plate supported at three corners under point load and (d) constant shear patch test

Table II. Convergence of central deflection and central bending moment for thick ($t/a = 0.1$) and thin ($t/a = 0.01$) situations in a simply supported (hard: $w = \theta_s = 0$) square plate under uniform loading. Results given for mesh orientations A and B shown in Figure 5

		$t/a = 0.1$		$t/a = 0.01$	
MESH	DOF	A*	B*	A†	B†
		Normalized central deflection			
2 × 2	7	5·1414	9·2607	5·0235	9·0212
4 × 4	28	4·7722	5·3477	4·5984	5·1294
8 × 8	112	4·4241	4·5252	4·2269	4·3184
16 × 16	448	4·3123	4·3302	4·1073	4·1271
32 × 32	1792	4·2826	4·2819	4·0753	4·0800
Analytic solution[17]		4·2728		4·0623	
		Central bending moment			
2 × 2	7	1·3542	3·2689	1·3542	3·2827
4 × 4	28	3·7573	4·4632	3·7723	4·4583
8 × 8	112	4·5081	4·7149	4·5115	4·7119
16 × 16	448	4·7261	4·7636	4·7136	4·7739
32 × 32	1792	4·7901	4·7661	4·7688	4·7860
Analytic solution[17]		4·79		4·79	

For normalized central deflection: *$w \times 10$; †$w \times 10^4$

Table III. Convergence of central deflection and central bending moment for thick ($t/a = 0.1$) and thin ($t/a = 0.01$) situations in a simply supported (soft: $w = 0$) square plate under uniform loading. Results given for mesh orientations A and B shown in Figure 5

		$t/a = 0.1$		$t/a = 0.01$	
MESH	DOF	A*	B*	A†	B†
		Normalized central deflection			
2 × 2	9	5·1557	9·3045	5·0237	9·0216
4 × 4	32	4·8427	5·4643	4·5592	5·1306
8 × 8	120	4·6088	4·7719	4·2292	4·3212
16 × 16	462	4·6350	4·7268	4·1125	4·1330
32 × 32	1824	4·6928	4·7723	4·0864	4·0918
Reference solution[17]				4·0623	
		Central bending moment			
2 × 2	9	1·3690	3·2844	1·3543	3·2828
4 × 4	32	3·8279	4·5563	3·7731	4·4592
8 × 8	120	4·6825	4·9312	4·5136	4·7144
16 × 16	462	5·0275	5·1077	4·7183	4·7791
32 × 32	1824	5·1725	5·1907	4·7787	4·7964
Reference solution[17]				4·79	

For normalized central deflection: *$w \times 10$; †$w \times 10^4$

Table IV. Convergence of central deflection and central bending moment for thick ($t/a = 0{\cdot}1$) and thin ($t/a = 0{\cdot}01$) situations in a clamped square plate under uniform loading. Results given for mesh orientations A and B shown in Figure 5

		$t/a = 0{\cdot}1$		$t/a = 0{\cdot}01$	
MESH	DOF	A*	B*	A†	B†
		Normalized central deflection			
2 × 2	7	4·6284	7·7073	4·5106	7·4432
4 × 4	24	2·8125	3·1095	2·6264	2·8566
8 × 8	104	1·8861	1·9508	1·6656	1·6985
16 × 16	432	1·6076	1·6424	1·3727	1·3811
32 × 32	1760	1·5344	1·5634	1·2946	1·2970
Analytic solution[17]		1·4990		1·2653	
		Central bending moment			
2 × 2	7	0·8207	2·0592	0·8207	2·0831
4 × 4	24	1·9297	2·4246	1·9562	2·4211
8 × 8	104	2·1796	2·3841	2·2097	2·3457
16 × 16	432	2·2476	2·3619	2·2670	2·3120
32 × 32	1760	2·2728	2·3506	2·2835	2·2980
Analytic solution[17]		2·31		2·31	

For normalized central deflection: *$w \times 10$; †$w \times 10^4$

Table V. Convergence of central deflection and central bending moment for thick and thin situations in clamped and simply supported (soft) circular plates under uniform loading.

		$t/R = 0{\cdot}1$		$t/R = 0{\cdot}01$	
ELEM.	DOF	$w_c \times 10^2$	$(M_x)_c^*$	$w_c \times 10^5$	$(M_x)_c^*$
		Clamped circular plate			
4	12	3·7668	6·9599	3·6950	6·9606
16	54	2·2352	7·7235	2·1657	7·7431
64	220	1·7882	7·9751	1·7186	8·0146
144	498	1·7023	8·0243	1·6326	8·0726
225	780	1·6774	8·0391	1·6077	8·0904
Reference solution[9,17]		1·6339	8·1250	1·5625	8·1250
		Simple supported circular plate (soft)			
4	17	7·2815	1·6400	7·2096	1·6402
16	62	6·7248	1·9427	6·6553	1·9449
64	236	6·5191	2·0279	6·4495	2·0319
144	522	6·4763	2·0437	6·4066	2·0487
225	810	6·4637	2·0484	6·3939	2·0536
Reference solution[9,17]		6·4416	2·0625	6·3702	2·0625

*For simply supported circular plate: *$(M_x)_c \times 10$

Table VI. Convergence of the central deflection at the two free corners ($w \times (Et^3/qa^4)$) for different skew angles in cantilever skew plates under uniform loading.

Mesh	DOF	20°		40°		60°	
		w_1	w_2	w_1	w_2	w_1	w_2
2×2	14	3·0093	2·6744	2·5112	1·3772	2·1821	0·4959
4×4	41	1·9701	1·7478	1·7478	0·8321	1·3882	0·2940
8×8	137	1·6032	1·1611	1·3950	0·6349	1·0800	0·2111
16×16	497	1·4802	1·0741	1·2610	0·5724	0·9521	0·1781
32×32	1889	1·4442	1·0517	1·2159	0·5554	0·9030	0·1672
DRM[10]	416	1·4269	1·0436	1·1789	0·5456	0·8435	0·1553
EL1[10,11]	472	1·4237	1·0421	1·1722	0·5441	0·8314	0·1538

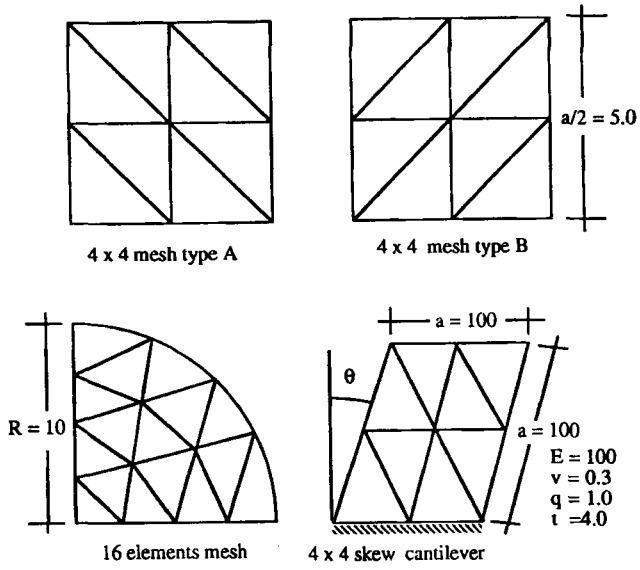

Figure 5. Description of meshes used for the analysis of square, circular and skew plates in Examples 4–6

EXTENSION TO SHELL ANALYSIS

The TLLL plate element presented in previous sections has been successfully combined with the simple linear plane stress triangle[1,2] for linear and non-linear shell analysis. The linear shell formulation is based in the standard facet shell approach. Two rotational degrees of freedom at the mid-nodes are kept which makes the formulation applicable to smooth shells only. The extension for kinked shell situations requires the introduction of a third drilling rotation at the non-coplanar nodes in the standard manner.[1,2] The non-linear shell formulation is based in Simo's shell theory.[12,13]

Figure 6 shows an example of the good performance of the TLLL element for non-linear shell analysis. The example corresponds to a pinned shallow cylindrical panel subjected to a central load. The geometry of the panel and the material properties are shown in Figure 6(a). Increasing

values of the applied load lead, eventually, to snap-through of the panel and reversal of its curvature. This problem is analysed using different meshes on one quadrant using symmetry conditions for two different thicknesses: $R/t = 200$ and $R/t = 400$. The load deflection paths for these cases are shown in Figure 6(a) and 6(b). Arc-length control was necessary in the second case due to the complexity of the different solution paths. Numerical results agree well in all cases with those reported in Reference 13.

Further evidence of the good performance of the TLLL element for shell analysis can be found in References 8 and 14.

DERIVATION OF A 6-DOF DISCRETE-KIRCHHOFF TRIANGLE

A simple Discrete Kirchhoff (DK) triangle can be derived from the TLLL plate element presented in previous sections simply by constraining the mid-side shear strains to a zero value. This

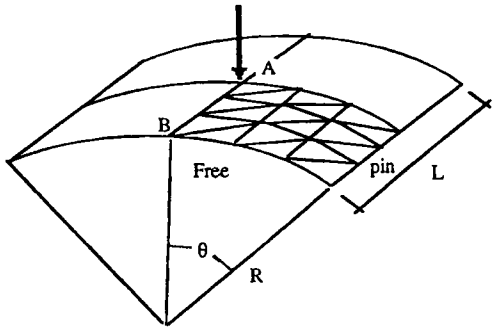

(a)

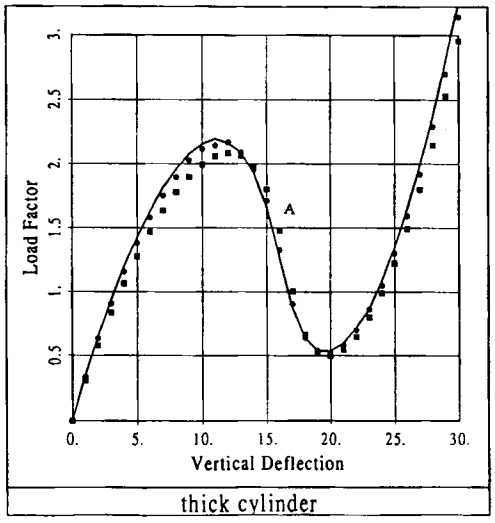

(b)

Figure 6. (a, b)

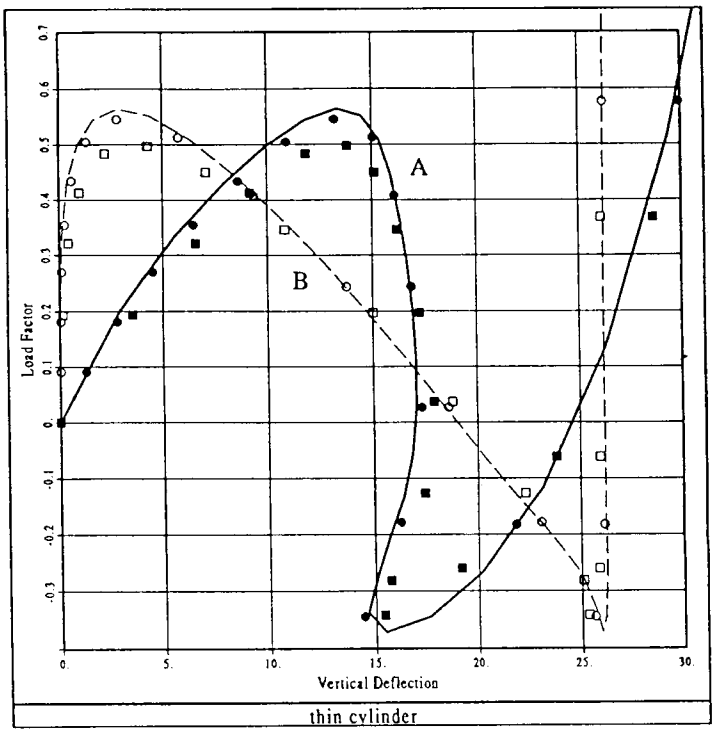

(c)

Figure 6. (a) Problem definition of the snap-through of a shallow hinged cylindrical panel. (b) Load–deflection path for the $R/t = 200$ case. Displacement control using 30 step levels are used. (c) Load–deflection path for the $R/t = 400$ case. Arc-length control was necessary in this case. Twenty step levels were used

provides the following relationship between the tangential rotation along a side ij and the two nodal deflection values corresponding to the side as

$$\theta_s^{ij} = \frac{w_j - w_i}{l_{ij}} \tag{16}$$

The resulting DK triangle termed DKTLL (for Discrete Kirchhoff Triangle with Linear deflection and Linear rotation fields) has only 6 DOF (three corner deflections and three normal rotations at the element mid-sides). The element stiffness matrix involves now the flexural contribution only (equation (13)). The explicit form of the modified curvature matrix is shown in Table VII. Note that a single point quadrature suffices for exact evaluation of $\mathbf{K}_b^{(e)}$ over straight side triangles with homogeneous material properties.

Remark 3. The stiffness matrix of the DKTLL element coincides with that of the well-known Morley's thin triangular plate element[15] and also with that of the HSM6 triangle proposed by Batoz and Dhatt (see pages 375 and 390 of Vols. II and III of Reference 4, respectively). However, the derivation presented here follows a completely different and simpler procedure. Also, note that the equivalent nodal load vector is different for each of these cases. The accuracy of the DKTLL element is identical to that shown for the TLLL element for thin plate situations in previous examples.

Table VII. Curvature matrix of the DKTLL triangle

$$\mathbf{B}_b = \begin{bmatrix} (a_{12}-a_{13}) & (a_{23}-a_{12}) & (a_{13}-a_{23}) & c_{12} & c_{23} & -c_{13} \\ (a_{13}-a_{12}) & (a_{12}-a_{23}) & (a_{23}-a_{13}) & b_{12} & b_{23} & -b_{13} \\ (d_{13}-d_{12}) & (d_{12}-d_{23}) & (d_{23}-d_{13}) & -2a_{12} & -2a_{23} & 2a_{13} \end{bmatrix}$$

$$a_{ij} = \frac{x_{ij}y_{ij}}{l_{ij}^2}, \qquad b_{ij} = \frac{x_{ij}^2}{l_{ij}}, \qquad c_{ij} = \frac{y_{ij}^2}{l_{ij}},$$

$$d_{ij} = \frac{x_{ij}^2 - y_{ij}^2}{l_{ij}^2}, \qquad x_{ij} = x_i - x_j, \quad y_{ij} = y_i - y_j$$

$$l_{ij} = (x_{ij}^2 + y_{ij}^2)^{1/2}$$

Remark 4. An extension of the DKTLL element to account for transverse shear deformation effects has been recently proposed by Van Keulen.[9] The approach is based on the introduction of three tangential shear strains at the element mid-side points which remain as additional variables. The final discretized system of equations is derived via a mixed-hybrid approach. Further details can be found in Reference 9.

CONCLUDING REMARKS

A simple 9-DOF triangular plate element with linear displacement and rotation fields has been presented. The element seems to satisfy all requirements defining an 'optimum' plate element valid for thick and thin situations. The drawback of having a different number of degrees of freedom per node as well as that of its slightly over-stiff behaviour are compensated by the simplicity of the element formulation. Preliminary results obtained show that the element is also very adequate for shell analysis.

Current research work aims to enhance the convergence behaviour of the element so that it can favourably compete with other low order triangles recently proposed for plate and shell analysis [3,5–7,9,10,16]

ACKNOWLEDGEMENTS

F. Zarate gratefully acknowledges the support of the Government of Mexico during the development of this work. F. Flores is supported by a fellowship from the Spanish Government; this support is gratefully acknowledged.

REFERENCES

1. O. C. Zienkiewicz and R. L. Taylor, *The Finite Element Method, McGraw Hill*, Vol. I, 1990; Vol. II, 1991.
2. E. Oñate, *Structural Analysis by the Finite Element Method*, CIMNE, Barcelona, 1995.
3. J. L. Batoz and I. Katili, 'On a simple triangular Reissner–Mindlin plate element based on incompatible modes and discrete constraints', *Int. j. numer. methods eng.*, **35**, 1603–1632 (1992)
4. J. L. Batoz and G. Dhatt, 'Modelisation des structures par elements finies', Vol. 2; *Poutres et Plaques*, 1990; Vol. 3: *Coques*, 1992, HERMES, Paris.
5. O. C. Zienkiewicz and D. Lefebvre, 'A robust triangular plate bending element of Reissner–Mindlin type', *Int. j. numer. methods eng.*, **26**, 1169–1184, (1988).
6. O. C. Zienkiewicz, R. L. Taylor, P. Papadopoulos and E. Oñate, 'Plate, bending elements with discrete constraints: new triangular elements', *Comput. Struct.*, **35**, 505–522 (1990).

7. E. Oñate, O. C. Zienkiewicz, B. Suarez and R. L. Taylor, 'A methodology for deriving shear constrained Reissner–Mindlin plate elements', *Int. j. numer. methods eng.*, **33**, 345–367 (1992).
8. F. Zarate, 'Nuevos elementos finitos para análisis de placas y láminas' *Ph. D. Thesis* (in Spanish), UPC, Barcelona, (to be submitted).
9. F. Van Keulen, 'On refined triangular plate and shell elements', *Ph.D. Thesis*, Technische Universiteit Delft, 1993.
10. F. Auricchio and R. L. Taylor, '3 node triangular elements based on Reissner–Mindlin plate theory', *Report No. UCB/SEMM-91/04*, Department of Civil Engineering, University of California, Berkeley, 1991.
11. Z. Xu, 'A thick–thin triangular plate element', *Int. j. numer. methods eng.*, **33**, 963–973 (1992).
12. J. C. Simo and D. D. Fox, 'On a stress resultant geometrically exact shell model. Part I. Formulation and optimal parametrization', *Comput. Methods Appl. Mech. Eng.*, **72**, 267–304 (1989).
13. J. C. Simo, D. D. Fox and M. S. Rifai, 'On a stress resultant geometrically exact shell model. Part III. Computational aspects of the non-linear theory', *Comput. Methods Appl. Mech. Eng.*, **79**, 21–70 (1990).
14. F. Flores and E. Oñate, 'A comparison of different finite elements based on Simo's shell theory', *Research Report No. 33*, CIMNE, Barcelona, 1993.
15. L. S. D. Morley 'On the constant moment plate bending element', *J. Strain Anal.*, **6**, 20–24 (1971).
16. O. C. Zienkiewicz, F. Auricchio and R. L. Taylor, 'Linked interpolation for Reissner–Mindlin plate elements', *Int. j. numer. methods eng.*, to be published.
17. S. Timoshenko and S. Woinowsky-Krieger, *Theory of Plates and Shells*, McGraw-Hill, New York, 1959.